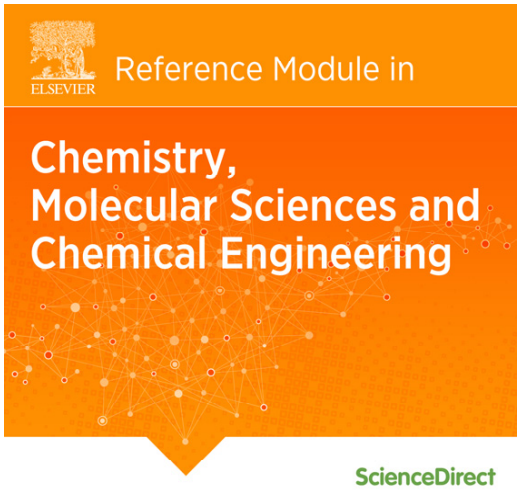

Phan N.T.N., Fletcher J.S. and Ewing A.G. (2014) Imaging Mass Spectrometry for Single-Cell Analysis. In: Reedijk, J. (Ed.) Elsevier Reference Module in Chemistry, Molecular Sciences and Chemical Engineering. Waltham, MA: Elsevier. 21-Nov-14 doi: 10.1016/B978-0-12-409547-2.11022-4.

Imaging Mass Spectrometry for Single-Cell Analysis

NTN Phan and JS Fletcher, University of Gothenburg, Gothenburg, Sweden; National Center Imaging Mass Spectrometry, Gothenburg, Sweden
AG Ewing, University of Gothenburg, Gothenburg, Sweden; National Center Imaging Mass Spectrometry, Gothenburg, Sweden; Chalmers University of Technology, Gothenburg, Sweden

Introduction

Single cells are the smallest living unit of any complicated biological system. In order to fully understand the biological complexity of an organism, it is very useful to study single-cell models. Traditionally, cell analysis was performed on large amounts of cells from which the data obtained were an average of the chemistry and behavior of all examined cells. However, heterogeneity exists not only among individual cells but also within a single cell. This results from variations in local abundance of a variety of biomolecules, complex cellular structures, and variations in cellular composition and behavior at different timescales. Localization of biomolecules in specific cellular regions can often be related to their functions in the biological processes occurring in the cells. Distribution information of cellular composition and molecular location thus has great potential benefit in biological, medical, and pharmaceutical research.

There are several main challenges for imaging single cells. First, the very small volume of a single cell requires analytical approaches with very high imaging resolution, smaller than the cell dimensions or relating to the size of the cellular process under study. Cell size typically varies from several micrometers to several hundreds of micrometers. The average size of mammalian cells is typically from 4 to 25 μm.[1] Second, sensitivity is a critical issue. Huge effort has been spent on technical developments particularly sampling efficiency improvement and interference limitations. Sensitivity also depends on the abundance of the analytes, which unfortunately is a trade-off with spatial resolution because the amount of detectable molecules diminishes with the smaller analyzed area or volume. In addition, sample handling is very important to preserve the cell samples in good condition for analysis. Changes in endogenous species and interferences of exogenous factors can cause artifacts in the results.

A wide range of analytical imaging techniques can be used for single cells including light microscopy, spectroscopy, and mass spectrometry.[2–7] However, imaging mass spectrometry (IMS) is the most favorable owing to its label-free and nontargeted approach, sufficient sensitivity for single-cell analysis (about attomole detection limit), high chemical specificity, and high accuracy for structural elucidation. IMS, specifically secondary ion mass spectrometry (SIMS), matrix-assisted laser desorption ionization (MALDI), and desorption electrospray ionization (DESI), has been rapidly and continuously developed with a long-term goal to image single cells. In this article, we introduce the technical advances and ongoing progress of IMS techniques particularly SIMS and MALDI and introduce the potential of DESI with regard to current and future single-cell imaging. Outstanding examples of single-cell imaging as well as sample preparation are also discussed.

SIMS Imaging of Single Cells

SIMS, a surface-sensitive technique, has to date been the most suitable mass spectrometry imaging platform for single-cell analysis owing to its easily achievable spatial resolution at the subcellular size level. The spatial resolution ultimately depends on the spot size of the primary ion beam but in reality is often limited by the available signal in each pixel. However, current developments in primary ion sources and matrix-enhanced SIMS have improved signal levels and, hence, the spatial resolution as well as the detectable mass range. The SIMS technique typically allows the detection of biological molecules up to 1500 Da., such as intact lipids, metabolites, lipid fragments, and elements.

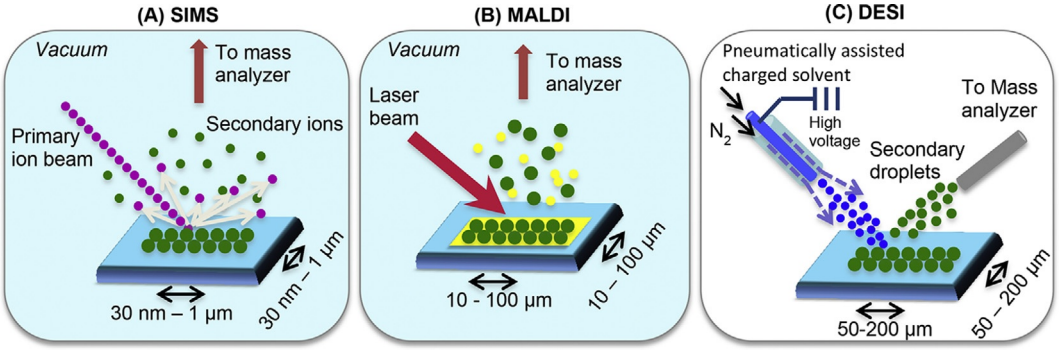

Figure 1 Ionization mechanisms of IMS techniques: SIMS, MALDI, and DESI. Green, analytes; yellow, matrix.

The ionization mechanisms for major imaging methods are shown in Figure 1. In SIMS, secondary ions are generated by the sputtering of the sample surface with a high-energy primary ion beam, usually between 5 keV and 40 keV. The secondary ions that are produced are extracted and separated in a mass analyzer. Mass analyzers can be time-of-flight (ToF), ion trap, and magnetic sector; however, the most commonly used for biological analysis is the ToF due to its capability to carry out parallel mass detection with good mass resolution and mass range. The most common method for imaging is microprobe mode. In microprobe mode, spatial resolution is determined by the beam size and the abundance of the ions detectable within the spot. Alternatively, but much less commonly, position-sensitive detectors are used in IMS introducing another concept of imaging acquisition – the microscope mode.[8,9] In this mode, an unfocused primary ion beam sputters a large area of the sample surface. The desorbed ions keep their original spatial position relative to their origin on the sample while they travel through the ion optics to the detector.

Development of new primary ion sources is one of the main assignments in instrumental development with the goal of obtaining spatial resolution as low as a few nanometers while minimizing the damage to the material, in other words, to improve the ion beam efficiency. With continuous development, various primary ion sources have been made available in the field. These can be atomic and diatomic (Cs^+, Ga^+, In^+, O_2^+, etc.), polyatomic (SF_6^+ and C_{60}^+), and liquid metal clusters (Au_n^+, Bi_n^+, etc.) or recently developed giant gas cluster ion beams (GCIBs) (Ar_n^+ and $(H_2O)_n^+$). These primary ion beams possess specific properties in terms of spatial resolution, detectable mass range, and sample damage. Detailed development and performance comparisons of the primary ion sources in SIMS can be found in the comprehensive literature.[10–16]

In addition to the advantages of being label-free and having molecular specificity, also obtained with any other mass spectrometric imaging techniques, SIMS provides chemical information with submicron spatial resolution. Furthermore, it is versatile and capable of ionizing almost all kinds of materials; therefore, modification of the sample surface with matrices in most cases is not necessary and can be detrimental to image resolution. SIMS is a highly surface-sensitive method, and, hence, any kind of contamination of the surface can produce faulty results. Sample preparation therefore often determines the success of the IMS analysis. This topic will be discussed in more detail when single-cell imaging is discussed.

As mentioned in the preceding text, sensitivity and spatial resolution of an analytical technique are the main criteria for single-cell imaging. SIMS accommodates these needs by two methodological regimes, *static* SIMS and *dynamic* SIMS.

Static SIMS

In static SIMS, the primary ion beam bombards the surface below a limited level called the static limit, typically taken as 10^{13} ions/cm^2, although this can be much lower for organic samples. Ideally, only 1% the material on the surface is impacted, ensuring that secondary ions represent the chemistry of the pristine sample. Because a focused primary ion beam is used, chemical information from the surface can be highly spatially resolved. This regime is used when the chemical composition on the material surface is of particular interest. Static SIMS has been increasingly applied in biological studies especially single-cell analysis to detect small ions below 1500 Da.

Lee[17] used static SIMS with a 25 keV Ga^+ liquid metal ion gun (LMIG) to validate the cytotoxicity of ZnO nanoparticles (NPs) commonly used in sunscreen products to HaCaT cells – a human skin equivalent cellular model. This was combined with confocal laser scanning microscopy to examine the physical structure of the ZnO NP-treated cells. ToF-SIMS imaging showed spatially resolved information about intracellular ZnO NPs, examining the $^{40}Ca/^{39}$ K ratio, which plays an essential function in living cells, phosphocholine membrane lipid fragments, and a fragment of glutathione, which is a typical antioxidant in cells. In particular, ^{64}Zn was found to progressively migrate into the inner cell with increasing concentration of ZnO NPs. It localized in the cytoplasm and nuclei at 50 µg ml^{-1} NPs or above. The $^{40}Ca/^{39}$ K ratio also increased with increasing ZnO NPs concentration underlying the activities of cell membrane channels Ca^{2+} and K^+ changed by the exposure of the NPs. In addition, stable isotope-labeled ^{68}ZnO NPs were also used as tracers for the incorporation of the NPs into different intracellular compartments. The study showed ZnO NPs can cause cell disruption and cell death.

To acquire relevant chemical and spatial images of heterogeneous single cells, one needs to choose suitable sample preparation methods to ensure the cells are kept intact in high vacuum condition for analysis. Different sample preparation protocols have been

investigated and comprehensively discussed in the literature.[18–20] The main protocols that have been widely used are freeze-drying, fixation, freeze fracture, frozen-hydrated preparation, etching by temperature, and etching by defocused etching gun such as C_{60}^+ or low-energy Ar GCIB.

Brison et al.[21] compared different protocols for sample preparation to image HeLa cells involving wash and dry with ammonium acetate, paraformaldehyde fixation, quick wash and snap freezing and then freeze-drying, trehalose vitrification, room temperature analysis and low temperature analysis at −90 °C, incubation with BrdU as cellular label, and paraformaldehyde fixation. The protocol that quick washing with ammonium acetate followed by snap freezing in liquid ethane and then freeze-drying seemed to show the best results where cellular morphology was preserved and chemical information located within the cells.

Chemical fixation with aldehydes is commonly used in histological studies for biological samples to preserve the microstructure of the sample due to the formation of intermolecular cross-linking proteins. Using ToF-SIMS with a Au_3^{2+} primary ion beam, Nagata et al.[22] investigated the influence of the glutaraldehyde fixation method on lipid imaging of multiple myeloma cell line U266. The cells were fixed with glutaraldehyde buffer followed by rinsing with ammonium acetate and stored at −80 °C. The analysis of the thawed fixed samples at room temperature showed that the cell morphology was maintained after fixation. Cellular fragmented ions such as PO_3^- and fatty acids were localized within the individual cell area. This suggested that fixation with glutaraldehyde did not affect the membrane phospholipids, and therefore, it could be applied to imaging lipids in single cells by SIMS.

One of the most commonly used sample preparation approaches is freeze-drying. The cells are transferred on to the substrate, rinsed to remove cell medium and salts, and then plunged frozen. The plunge freezing minimizes the ice crystallization in the sample. The cells are then allowed to dry in a vacuum chamber for several hours. The sample is analyzed at room temperature, which makes it simple and easy for the manipulation. However, there is a risk of morphological change of the cells, and chemical migration can be high during the drying process, causing artifacts in analysis. Freeze fracture and frozen-hydrated preparation approaches are considered the safest ways to preserve the cell nature. Typically cells, after plunge freezing, are kept frozen during the analysis. Freeze fracture uses a special device to fracture the sample in the vacuum into two parts with the hope of exposing the outer and inner cellular compartments for analysis. Frozen-hydrated analysis typically requires the use of an etching gun or slowly increasing the temperature to remove the top ice layers covering the cells. Both strategies maintain the cell morphology and prevent contamination, which possibly occurs on top of the cells; however, the sample handling is elaborate and time-consuming. An interesting example of these strategies is imaging membrane lipids on mating *Tetrahymena thermophila* by Kurzcy et al.[23] Two complementary cell strains were induced to mate and were prepared for analysis using the freeze fracture and frozen-hydrated methods. In the intact plasma membranes of tightly bound *Tetrahymena*, the lipids, notably the headgroup of lamellar-shaped phosphatidylcholine (PC) at m/z 184, diminished in the mating junction where that of conically shaped 2-aminoethylphosphonolipid (2-AEP) at m/z 126 was more intense (**Figure 2(a)–2(c)**). Importantly, changes in membrane domains observed previously[24] were now examined as a function of junction stability, and it was concluded that the cell membranes formed junctions prior to changes in lipid composition.

Dynamic SIMS/NanoSIMS and Multiple-Isotope Imaging Mass Spectrometry

In contrast to static SIMS, dynamic SIMS utilizes a high-dose density of primary ions (above 10^{13} ions/cm^2) to erode the surface. Dynamic SIMS instruments usually use quadrupole or magnetic sector mass analyzers as these are compatible with a continuous, d.c., primary ion beam. Dynamic SIMS is most commonly used in the semiconductor industry. With time, the top surface layers can be removed completely. The primary ion beam in dynamic SIMS is normally monoatomic, which causes intensive fragmentation; therefore, the regime is mainly used to analyze atomic and small fragmented ions. However, the resulting highly focused ion beam yields very high spatial resolution (<50 nm). The use of reactive species such as cesium and oxygen also enhances secondary ion formation of negative and positive ions, respectively, allowing sufficient signal to be detected despite the small spot size. Dynamic SIMS has been used widely for depth profiling of single cells, in which the primary ion beam erodes the sample layer by layer and provides one spectrum of the whole sample area. When using this method, lateral spatial chemical information is compromised in order to obtain information as a function of depth. The depth profiling method will not be discussed further here as it is beyond the scope of this article.

Dynamic SIMS has also been used to image elemental ions at subcellular resolution. In those experiments, the microscope mode was traditionally used; however, only one ionic species at a time could be detected; thus, it was called ion microscopy. Significant work in this area was done by Chandra and Morrison et al., who extensively applied ion microscopy to different research areas and developed methodology such as freeze fracture and freeze-drying sample preparation, isotope tracking, and 3-D imaging for cells using ion microscopy.[25–28] The recently developed NanoSIMS instrument by Cameca is a development of ion microscopy but using a focused ion beam in the microprobe mode. Since its introduction to the SIMS community, the NanoSIMS has opened increasing accesses for SIMS to biological studies especially single-cell analysis. In the NanoSIMS instrument, the incidence of the primary ion beam is normal to the sample surface (typically 45° in other SIMS instruments) and so coaxial with the secondary ion path. The focusing lens of the primary ions and extraction lens of secondary ions therefore have shortened focal length. This results in significant reduction of aberration, and the primary ion beam can be focused into a very small diameter. Very small probe sizes, 30 nm, can be obtained when using Cs ion beams. Furthermore, the NanoSIMS exhibits several superior properties compared with standard magnetic sector-based depth profiling SIMS instruments, particularly high mass resolution, parallel detection of up to

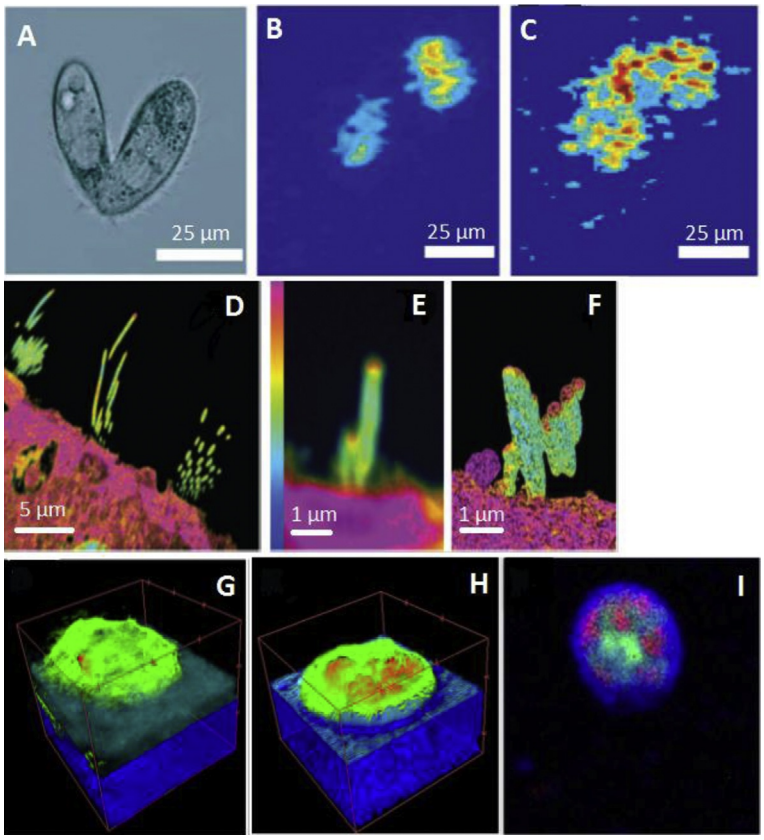

Figure 2 Imaging of lipids, proteins in single cells using SIMS IMS. (a–c) Imaging of a mating *Tetrahymena* cell pair. (a) Microscopic image; (b–c) SIMS selected ion images: (b) PC at m/z 184, (c) 2-AEP at m/z 126. Scale bars are 25 μm (Adapted from Kurczy et al.[23]). (d–f) Incorporation of ^{15}N into mouse hair cells studied by NanoSIMS, day 56. (d) Ratio image of $^{12}C^{15}N$:$^{12}C^{14}N$ (m/z 27: m/z 26) of utricle shows low incorporation in stereocilia; (e) $^{12}C^{15}N$:$^{12}C^{14}N$ ratio image of cochlear inner hair cell; (f) 3-D reconstruction from 450 ratio images of cochlear inner hair cells (Adapted from Zhang et al.[34]). (g–i) 3-D reconstruction of *Tetrahymena* cells. (g) TiO_2 nanoparticle-treated cell; (h) control cell. Cell membrane at m/z 184 in green, silicon substrate at m/z 168 in blue, and water ice in cyan. Red in G is $[TiO]^+$ signal at m/z 64, and red in H is the cell vacuoles at m/z 213; (i) 2-D image at m/z 101.05 in red, at m/z 198.95 in blue, and at m/z 158.95 in green. Image sizes are 128×128 μm^2, 128×128 pixels. Adapted from Angerer, T. B.; Fletcher, J. S. *Surf. Interface Anal.* **2014**.

seven ions, and high secondary ion transmission.[29,30] The NanoSIMS enables dynamic SIMS analysis with high spatial resolution less than 50 nm, which is extremely challenging for other dynamic SIMS instruments.

Different sample preparation protocols have been developed and used for the analysis of samples using the NanoSIMS, which fall into three main categories: chemical fixation, cryogenic fixation, and freeze-drying. For larger molecules such as proteins (imaged using the CN^- signal), chemical fixation is the regular choice.[31,32] The standard procedure is that samples are fixed and sectioned in an ultramicrotome to obtain slices of thickness up to 500 nm. The sample sections are then subjected to TEM measurement and subsequently to NanoSIMS analysis. TEM imaging is very useful for locating the areas of interest on the samples. On the other hand, cryogenic fixation is essentially used for small molecules and easily diffusible molecules. Freeze-drying is another choice that can limit the diffusion of biomolecules during the drying process in vacuum at low temperature.

A method called multiple-isotope imaging mass spectrometry (MIMS) has been developed to complement and enhance NanoSIMS analysis. The method allows imaging and quantification of molecules labeled with nonradioactive stable isotopes at subcellular spatial resolution (<50 nm). The use of nonradioactive isotopes does not affect the biochemical reactions in the organism and therefore enables the *in vivo* measurement of a particular biological process. The isotopic elements are integrated into the body or organism typically by food, injection, or suitable cellular medium. The samples with isotope labeling are then analyzed to obtain the isotopic atomic images and isotope abundance such as $^{13}C/^{12}C$ and $^{15}N/^{14}N$. For quantification, the isotope abundance is compared with natural abundance in a control sample. Lechene and coworkers[30] have pioneered the application of MIMS with the NanoSIMS. Several prominent examples of this technique include tracking and quantifying stem cell division in mammalian intestine and lipid metabolism in individual lipid droplets, which presents the abundance of enterocytes in *Drosophila* intestine[33], and quantifying the protein synthesis in hair-cell stereocilia of the inner ear of frogs and mice *in vivo*.[34] **Figure 2(d)–2(f)** is an example showing 2-D and 3-D images of the incorporation of the isotope ^{15}N into mouse hair cells. More recently, they have studied the frequency and the sources of generation of new mammalian heart cells.[35] The authors administered ^{15}N thymidine to mice of different ages for 8 weeks and used MIMS with a Cs^+ primary ion gun to localize the isotopic tracers. The isotope

incorporation was detected by measuring the increase of the ^{15}N:^{14}N ratio above the natural ratio (0.37%). It was possible to highly resolve the cardiomyocyte cell border and to distinguish the sarcomeres and the adjacent stromal cells. ^{15}N labeling was observed to be concentrated in the nuclei. The results showed that ^{15}N labeling in the nuclei, which corresponds to DNA synthesis during postnatal development, decreased with aging. Furthermore, combined with tracking double-transgenic MerCreMer/ZEG cardiomyocytes, which are labeled with green fluorescent protein expression during their generation period, MIMS could be used to identify new ^{15}N cardiomyocytes generated from DNA synthesis primarily by the preexisting cardiomyocytes, not by the cardiac progenitors. The rate of renewal was about 0.76% per year in a young adult mouse under normal homeostatic conditions.

Spatial distribution of lipids in the plasma membrane regulating lipid signaling and biological cellular processes has been evident. Distinct domains of different lipids on the plasma membrane have been investigated.[24,36,37] Imaging these complex nano- to microdomains requires analytical techniques with outstanding spatial resolution and reliability to visualize their compositional structures. Frisz et al.[38] provided excellent evidence for domains of sphingolipids in the plasma membrane of fibroblast cells using NanoSIMS and ^{15}N-labeled sphingolipids and ^{13}C-labeled fatty acids. The ^{13}C fatty acids were used here to control artifacts from cell topography. The cells were cultured in a medium with ^{15}N sphingolipid precursors and then with ^{13}C fatty acids. Cells adhered onto specified substrates were rinsed to remove cell medium, followed by drying for SIMS analysis or further fixation with glutaraldehyde. Before analysis with the NanoSIMS, the samples were coated with a thin layer of iridium to prevent any charging effects. In this study, numerous sphingolipid microdomains of roughly 200 nm diameter were identified. These microdomains clustered to form larger domains from 5 to 10 μm diameter on the cell membrane especially at the soma. Considering other factors such as cholesterol depletion and cytoskeletal disruption, it was likely that the first did not affect sphingolipid domain formation significantly while the latter directly decreased sphingolipid domains. The study therefore categorized sphingolipid separately from lipid rafts.

MIMS is also very useful in medical research in which it plays as an exploratory tool for the distribution of drugs after administration into the organism body. MIMS can be used to investigate the mechanism and the sites of action of the drugs at subcellular level. One of the examples in this area is multimodal imaging of the distribution of the ^{15}N-labeled platinum-based anticancer drug cisplatin in human colon cancer cells using MIMS and fluorescence microscopy.[39] Monolayers of colon cancer cells were adhered on the substrate where they were treated with ^{15}N-labeled cisplatin. The cells were then embedded in resin and subsequently sectioned for MIMS analysis. Different cellular compartments were identified based on different atomic secondary ion images including the cytoplasm, nucleus, nucleolus, and chromatin. Cisplatin was found to accumulate in sulfur-rich and phosphorous-rich aggregates inside the cytoplasm and nucleolus, where the drug was believed to bind to S-ligands and DNA. In addition, the drug also had high affinity to N-ligands and acidic environments. The affinity of the drug towards S-rich, N-rich, and acidic organelles could be the basis for the mechanism of action of the drug and the cell resistance mechanism.

Three-Dimensional Imaging SIMS of Single Cells

Three-dimensional IMS – SIMS, MALDI, or DESI – has been an emerging label-free imaging modality attracting huge interest in the biological and medical communities.[6,40–42] This modality provides a three-dimensional distribution of the molecular species within an organism.

As discussed in the preceding text, various primary ion sources have been introduced for SIMS. Since the introduction of polyatomic ion guns, especially C_{60}^+, conventional ToF-SIMS instruments have utilized a combination of static and dynamic SIMS for 3-D imaging. In this approach, a finely focused analysis beam commonly an LMIG is used to statically image the sample, and then a nonfocused etching beam such as a polyatomic ion gun is used to dynamically remove the damaged layer to prepare a fresh new surface for the next cycle. The analysis can be continued effectively etching through the sample, and chemical images of all the layers can be stacked together to create a 3-D chemical image. Dual beams or a single beam used for both analyzing and etching functions can be used. The most recently developed instrument for this approach, the 3-D Imager J105 from Ionoptika, however, employs a C_{60}^+ ion gun to dynamically erode the image, and 2-D images are recorded along the depth of the sample. Unlike the other dynamic SIMS instruments, the J105 uses a ToF mass analyzer, and the use of the C_{60}^+ gun enables the detection of molecular ions up to about m/z 1000 Da.

Fletcher and coworkers[43] used this approach to image through single cells. The authors examined sample preparation approaches including fixing with formalin, freeze-drying, and nonfixing and frozen-hydrated samples to image HeLa cells using the J105. For frozen-hydrated samples, a freeze fracture device called a *mousetrap* was used to fracture the sample apart, exposing clean cells for analysis. A 40 keV C_{60}^+ beam was used to obtain a series of images with the ion fluence exceeding the static limit. The frozen-hydrated method preserved the localization of many cellular components. Specific cellular markers, the headgroup of the membrane lipid phosphatidylcholine at m/z 184 and the DNA base adenine at m/z 136, were used for 3-D image reconstruction. Subcellular compartments such as nuclei and endoplasmic reticulum were clearly visualized.

Another example is the work by Brison et al.[44] who used the ION-ToF instrument with dual beams 25 keV Bi_3^+ as an analysis beam and a 10 keV C_{60}^+ ion source as the etching beam to image HeLa cells. The cells were incubated with a nuclear marker bromodeoxyuridine (BrdU), fixed with paraformaldehyde, and then washed and air-dried before analysis. The etching step with C_{60}^+ proved very useful to remove the damage or smearing during air-drying sample preparation. Different acquisition modes were checked with regard to the ion image qualities. The burst mode, in which the primary analysis beam is a burst of short pulses of primary ions, was used as it showed good compromise between spatial resolution and mass resolution. The data showed clearly

that the location of nuclei marked with BrdU and other subcellular regions represented by cellular markers like CN^-, CNO^-, and $C_xH_yO_z$ could be distinguished in 3-D.

Angerer et al. recently reported the 3-D distribution of TiO_2 nanoparticles inside single *Tetrahymena* cells.[45] The cells were fed with TiO_2 NPs, washed, and analyzed frozen-hydrated. A J105 equipped with the 40 keV C_{60}^+ beam was used for analysis. Cellular markers specific for different cellular compartments were detected such as phosphocholine headgroup at m/z 184.1 from the plasma membrane and at m/z 212.8 from the food vacuoles. The study showed 3-D images of *Tetrahymena* (shown in **Figure 2(g)–2(i)**), indicating that TiO_2 nanoparticles incorporated into the cells through the mouth and accumulated in the vacuoles.

MALDI Imaging of Single Cells

Matrix-assisted laser desorption/ionization imaging mass spectrometry (MALDI-IMS) has played a very important part in the imaging technologies for organic compounds. The technique provides spatially resolved information of the analyzed ions over a mass range from several hundreds to several tens of thousands Da., which covers a variety of biomolecules including intact lipids, peptides, proteins, and polymers. The principle of MALDI is demonstrated in **Figure 1(b)**. Typically, in a MALDI imaging experiment, a sample is coated with a thin homogeneous layer of organic matrix solution before analysis. The role of the matrix solution is important for the soft ionization of the analyzed biomolecules. The solution helps extract the biomolecules from the sample surface to mix and cocrystallize with the matrix molecules when the solution evaporates. The matrix then directly absorbs the energy from the irradiated laser. MALDI is a *soft* ionization technique in that there is little fragmentation of molecules during ion formation. Ions are normally singly charged and can include peptides and proteins. The lasers used in MALDI are UV or IR lasers; the most common are N_2 at wavelength 337 nm and Nd:YAG at wavelength 355 nm.

Spatial resolution is one of the most critical factors determining the possibility of single-cell imaging by MALDI-IMS. Generally the achievable spatial resolution on a commercial MALDI instrument is about 20 μm (although some are quoted at 10 μm), which is the smallest spot size of the laser. Spatial resolution is primarily dependent on laser beam size and matrix crystal size. Modifying either of these factors should improve the spatial resolution for single-cell imaging. There have been various ways to narrow the beam size. With a given laser on a commercial MALDI, oversampling can be used.[46] The laser completely ablates the overlapping part of two adjacent spots; therefore, significant signal only comes from the fresh adjacent area, which is smaller than the spot size. This strategy has a long analysis time, however, as it requires complete ablation of material. An alternative is the use of the microscope acquisition mode with a position-sensitive detector like that used in SIMS although this is not commercially available.[47] Another approach is an instrumental development where the transmission geometry is altered so the laser irradiates from the back side of the sample placed on a transparent substrate.[48] With this geometry, the beam size can be focused down to 1–2 μm. Spengler has used an atmospheric MALDI interface to produce a coaxial laser/ion extraction system where the laser focal length can be greatly reduced for improved spatial resolution.[49]

Sample purity and homogeneity are critical in obtaining high-spatial resolution images. Matrix crystal size modification, sample washing, matrix application, and surface modification have all been examined in some detail and show promising improvements aimed at improved spatial resolution. Washing is recommended to remove small and easily diffusible molecules (salts, glycerides, and lipids) when high-mass species are of interest such as peptides and proteins. In this case, cold washing should be used to prevent the delocalization of the biomolecules while removing the interferences. The choice of matrix and how to apply it on the sample surface can also affect the imaging results. Different matrices have different crystal sizes; for example, crystallized 2,5-dihydroxybenzoic acid (DHB) is larger than alpha-cyano-4-hydroxycinnamic acid (alpha-CHCA). Various methods of matrix application have been developed for both manual and automatic depositions, including the use of an airbrush, sprayer, sublimation, and inkjet printer.[50,51] Among those, sublimation appears to show limited diffusion of analytes, homogeneous matrix coating, and significantly smaller crystal size compared to wet deposition methods. In addition, investigation of surface modification noticeably with nanoparticles (NPs) as an alternative for the standard organic matrix has been extensively carried out.[52] This surface modification falls into a new technical platform – surface-assisted laser desorption/ionization (SALDI). Nanoparticles of various materials with diameters from 2 nm to less than 100 nm have been shown to efficiently absorb the laser energy, which then assists the ionization of biomolecules. The nanosize of these particles offers the possibility to obtain high spatial resolution for subcellular analysis if a sufficiently small laser beam spot is used and there is sufficient sensitivity to detect extremely small numbers of biomolecules. Although SALDI with nanoparticles has not been applied for imaging across single cells to date, imaging tissue samples at cellular resolution has been successfully performed.[53,54]

To improve the spatial resolution of MALDI measurements of single cells, Bouschen et al.[55] modified the matrix deposition procedure and imaged human renal carcinoma cells using the microscope acquisition mode. Various methods of matrix deposition were examined including dried-droplet preparation, pump spray, nebulizer spray with nonreactive gas stream, and sublimation followed by recrystallization. The nebulizer spray showed good compromise between the incorporation of analytes and matrix crystal and the delocalization of analytes on the surface. The nebulizer spray method was successfully applied for imaging human renal cancer cells. Cell markers within m/z 500–5000 were detected. On the other hand, the sublimation/recrystallization experiments, in which the matrix was sublimated onto the sample surface and then recrystallized in a saturated water environment to increase the integration of analytes into matrix crystals, provided high lateral resolution, as low as 2 μm. The method was only demonstrated on a peptide mixture in this work; however, it is promising for subcellular imaging applications.

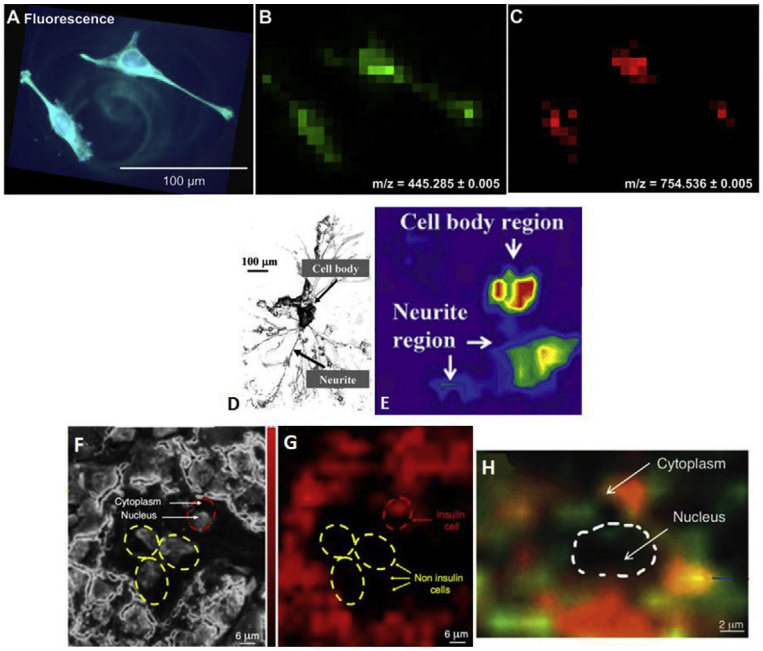

Figure 3 Imaging of lipids, peptides, and proteins in single cells using MALDI-IMS. (a–c) Imaging of HeLa cells. (a) Optical fluorescence image; (b–c) MALDI-selected ion images (spatial resolution ~7 μm): (b) Fluorescence staining agent of cell membrane, (c) $[PC(32:1)+Na]^+$ (Adapted from Schober et al.[56]). (d–e) Imaging of single cerebral ganglion neuron. (d) Optical image; (e) MALDI image peptide at m/z 4617 (spatial resolution <50 μm) (Adapted from Rubakhin et al.[57]). (f–h) Imaging of insulin-immunoreactive pancreatic cells. (f) Optical image of insulin-containing cells (red outline) and non-insulin-containing cells (yellow outline); (g–h) MALDI images: (g) insulin cells with mass tag at m/z 323 in red color; (h) localization of synaptophysin and insulin (laser spot size 2 μm), synaptophysin with mass tag at m/z 333 in green, insulin at m/z 323 in red, and colocalization of synaptophysin and insulin in yellow. Adapted from Thiery-Lavenant, G.; Zavalin, A. I.; Caprioli, R. M. *J. Am. Soc. Mass Spectrom.* **2013**, *24*, 609–614.

Schober et al. have also improved spatial resolution in MALDI to image metabolites in single HeLa cells.[56] Coupling atmospheric pressure MALDI to a Fourier transform orbital trapping mass analyzer produced imaging data with high spatial resolution (7 μm) and high mass resolution (100 000 at m/z 200). The cells were cultured on ITO glass, washed, and fixed by glutaraldehyde, followed by nebulizer spray with DHB. Different biomolecules including cholesterol, glycerides, phospholipids, and sphingomyelin were observed and identified within a cell. The microscopic and MALDI selected ion images of HeLa cells are shown in Figure 3(a)–3(c).

Rubakhin and coworkers[57] developed the protocols to spatially profile neuropeptides in a single ganglion neuron of *Aplysia californica* using MALDI with the spatial resolution less than 50 μm. The sample preparation was examined regarding the cell morphology, peak intensities of peptides, and salt adducts. The neurons were fixed by paraformaldehyde, stabilized by 50/50 glycerol/artificial seawater, frozen, covered with matrix α-CHCA, and quickly dried on a hot place surface for less than 30 s. The results showed that single neurons could be imaged with MALDI without neuropeptide relocation. An intense signal was observed for the peptide at m/z 4617 in the cell body, whereas no signal was observed for the peptide in the neurite (Figure 3(d) and 3(e)).

As mentioned in the preceding text, the backside MALDI geometry significantly improves spatial resolution, down to 1–2 μm. With a fixed laser wavelength, the beam size and hence spatial resolution decrease with increasing focusing angle of the laser beam. The conventional geometry in which the laser source is located in front of the sample, however, restricts enlarging the focusing angle because it interferes with the ion extraction field. Placing the laser source on the back of the sample offers maximum focusing angle (axial to the ion path) while the ion extraction field is undisturbed; therefore, the highest possible spatial resolution can be achieved. This modification has been applied to visualize the antigens insulin and synaptophysin within single human pancreatic endocrine cells (Figure 3(f)–3(h)).[58] The antigens were immunolabeled to mass tag-coupled antibodies, which released the mass tags of a specific m/z under laser irradiation for MALDI detection. From the results, two cell types were identified based on the localization of their specific antigens. Intracellularly, colocalization of the proteins insulin and synaptophysin was observed within a beta cell, while the proteins synaptophysin and somatostatin were distributed in different cellular compartments in a delta cell. The work can be further developed to study the immunoreactivities of different cell types.

For 3-D imaging with MALDI, the sample is typically sectioned into thin sections with suitable thickness. A series of selected sections are deposited with matrix before MALDI analysis. The individual images are then aligned and reconstructed from 2-D images of all the sections by coregistering with microscopic images or fiducial markers.[59,60] This step can be done by commercial or home-built software.[41,61] Although current developments reach subcellular resolution, 3-D MALDI imaging on single cells has not

Table 1 Comparison of technical performances of IMS techniques SIMS, MALDI and DESI

Technique	*Ionization sources*	*Ionization condition*	*Spatial resolution*	*Sensitivity*	*Mass range (Da)*	*Subcellular imaging capability*
Static SIMS	Polyatomic, cluster primary ions ($<10^{-13}$ ion/cm^2), for example, Bi_3^+, C_{60}^+, Au_3^+, and Ar_{2000}^+	Vacuum	>100 nm	amol	Molecules (1–1500)	Yes (routine)
Dynamic SIMS	Monoatomic, diatomic primary ions ($>10^{-13}$ ion/cm^2), for example, Cs^+, O^+, O_2^+	Vacuum	<50 nm	amol	Elements (1–250)	Yes (routine)
MALDI	Laser, for example, Nd:YAG 355 nm, N_2 337 nm	Vacuum	1–2 μm	fmol	Molecules (1–100 K)	Yes (exceptional circumstances)
DESI	Charged solvent, for example, MeOH, H_2O, ACN	Ambient	~50 μm	fmol	Molecules (<30 K)	Not yet!

Reproduced from Kollmer, F. *Appl. Surf. Sci.* **2004**, *231–232*, 153–158; Takats, Z.; Wiseman, J. M.; Cooks, R. G. *J. Mass Spectrom.* **2005**, *40*, 1261–1275.

been presented to date because of either the need of surface modification before analysis or the insufficient depth resolution of MALDI imaging for single cells.

'Omics' of Single Cells

Mass spectrometric-based, single-cell imaging is being increasingly applied in the 'omics' area. Proteomics, peptidomics, metabolomics, and lipidomics are omic fields of study aimed at understanding the functions of proteins, peptides, metabolites, and lipids, respectively, in a biological system. Omic studies of organisms such as fungi, bacteria, animal tissues, and single cells were originally carried out using NMR or MS with electrospray ionization MS.[62–64] MS gives high sensitivity and selectivity and enables coupling to separation or microfluidic devices. Samples are normally extracted and concentrated in suitable solution for analysis. For cell analysis, the data obtained are the average values of the collection of cells, which does not account for the heterogeneity within a cell and among individual cells. The distributional information of the analytes, which can be closely related to their biological functions, is therefore lost. The rapid development of imaging mass spectrometry, especially SIMS and MALDI, for single-cell imaging offers the possibility to explore the interior of cells, while the distribution of the biomolecules remains intact in the cellular compartments. IMS covers a wide mass range of the 'omics' from small metabolites with m/z several Da to huge proteins with m/z several tens of thousands Da. Technical performances of different IMS techniques are compared in Table 1.[12,65–69] SIMS is well suited for imaging small metabolites and intact lipids with spatial resolution down to several hundred nanometers. The NanoSIMS, using MIMS, is applicable to most kinds of molecules including lipids, peptides, and proteins with even better resolution 50 nm provided that a specific isotopic label can be incorporated. On the other hand, MALDI is well suited for the detection of peptides and proteins although the sensitivity for protein detection generally needs further improvement. Applications of MALDI for profiling and imaging of peptides and proteins at cellular spatial resolution (5–20 μm) are prevalent.[70–72] With rapid developments in the area of spatial resolution, ambient ionization IMS also promises potential applications for the lipidomics and metabolomics of single cells.

Future Perspectives

DESI and Nano-DESI

A current emerging trend in mass spectrometry is ambient MS in which analytes from the sample are ionized at atmospheric pressure before being extracted into the high vacuum chamber of the mass spectrometer for mass separation and detection. DESI, for which the ionization mechanism is shown in Figure 1(c), is one of the well-known techniques in this category. In DESI, charged droplets produced by a pneumatically assisted electrospray emitter are directed to the sample surface. The initial charged droplets form a thin film that helps extract the analytes on the surface. The thin film is then splashed into numerous secondary microdroplets (0.8–3.3 μm size with the electrospray velocity ~120 m s^{-1}) containing the extracted analytes by the following arriving charged droplets.[69,73] The microdroplets then undergo solvent evaporation and subsequently produce dry ions while traveling to the inlet of mass spectrometer. Spatial resolution was originally around 200 μm; however, modifications can be made to improve to ~50 μm.[74] Another version of DESI, called nanospray DESI or nano-DESI, has potential for higher-spatial-resolution imaging. Instead of splashing away the microdroplets into the MS inlet by collision with the primary charged droplets, nano-DESI uses two-piece nanospray capillaries, which are connected together by a solvent bridge.[75] The bridge is in contact with the sample surface in order to collect analytes from the sample. The analytes together with solvent are then self-aspirated into the MS inlet when a voltage is applied between the capillary inlet and the MS inlet. This configuration improves the transport efficiency of analytes and eliminates the splashing. This configuration is beneficial to spatial resolution. A resolution of 12 μm was reported for imaging of rat brain tissue.[76]

DESI and nano-DESI so far have not been applied to cell imaging although a procedure for cell culture analysis has been developed.[77] However, ambient imaging might allow data acquisition from live samples at the cellular level. A lot of issues need to be worked out in these experiments, however.

New Ion Sources and Cells

The advent of the GCIBs will invariably change the perspective for SIMS imaging of cells. The larger size of the clusters coupled to higher energy beams provides less fragmentation, allowing simpler spectra of molecular ions.[78] A key feature here will be to reduce the beam spot size from a few micrometers to a few hundred nanometers. When that occurs, impressive images of lower abundance molecules across cell surfaces and in the inner structure will be obtained. A great deal of work is currently ongoing to make mixed cluster beams to get the best of all worlds, and this will also be a major part of the future of single-cell chemical imaging.

3-D and NanoSIMS Targets at the Cell and Subcellular Level

The largest practical difference between the 'gold standard' of confocal fluorescence imaging and IMS is the ability to really get 3-D images of live cells. While it will be some time before someone develops the means to carry out IMS on live cells, likely something like DESI at higher spatial resolution and a way to keep the cells hydrated and healthy, schemes to carry out 3-D imaging are already available. These are discussed in the preceding text, and a great deal of work is ongoing in the field to improve and develop these. The NanoSIMS is an incredibly powerful technology that has just begun to scratch the surface of the single-cell imaging world. The future here is going to be determined by how many life scientists can be convinced to try this technology to answer their questions and how many can get access to it. Smaller ion beams and more energy to get significant signals from molecules in the smallest regions of cells will lead to not only single-cell analysis but also single and eventually suborganelle analysis.

References

1. Dittami, G. M.; Sethi, M.; Rabbitt, R. D.; Ayliffe, H. E. *J. Vis. Exp.* **2012**, 1–7.
2. Wu, B.; Becker, J. S. *Int. J. Mass Spectrom.* **2011**, *307*, 112–122.
3. Cialla, D.; Deckert-Gaudig, T.; Budich, C.; Laue, M.; Moller, R.; Naumann, D.; Deckert, V.; Popp, J. *J. Raman Spectrosc.* **2009**, *40*, 240–243.
4. Corezzi, S.; Urbanelli, L.; Cloetens, P.; Emiliani, C.; Helfen, L.; Bohic, S.; Elisei, F.; Fioretto, D. *Anal. Biochem.* **2009**, *388*, 33–39.
5. Chwiej, J.; Adamek, D.; Szczerbowska-Boruchowska, M.; Krygowska-Wajs, A.; Wojcik, S.; Falkenberg, G.; Manka, A.; Lankosz, M. *J. Biol. Inorg. Chem.* **2007**, *12*, 204–211.
6. Fletcher, J. S. *Analyst* **2009**, *134*, 2204–2215.
7. Gessel, M. M.; Norris, J. L.; Caprioli, R. M. *J. Proteomics* **2014**, *107C*, 71–82.
8. Kiss, A.; Jungmann, J. H.; Smith, D. F.; Heeren, R. M. *Rev. Sci. Instrum.* **2013**, *84*, 013704.
9. Schueler, B. W. *Microsc. Microanal. Microst.* **1992**, *3*, 119–139.
10. Kotter, F.; Benninghoven, A. *Appl. Surf. Sci* **1998**, *133*, 47–57.
11. Davies, N.; Weibel, D. E.; Blenkinsopp, P.; Lockyer, N.; Hill, R.; Vickerman, J. C. *Appl. Surf. Sci.* **2003**, *203–204*, 223–227.
12. Kollmer, F. *Appl. Surf. Sci.* **2004**, *231–232*, 153–158.
13. Touboul, D.; Kollmer, F.; Niehuis, E.; Brunelle, A.; Laprevote, O. *J. Am. Soc. Mass Spectrom.* **2005**, *16*, 1608–1618.
14. Weibel, D.; Wong, S.; Lockyer, N.; Blenkinsopp, P.; Hill, R.; Vickerman, J. C. *Anal. Chem.* **2003**, *75*, 1754–1764.
15. Ninomiya, S.; Nakata, Y.; Honda, Y.; Ichiki, K.; Seki, T.; Aoki, T.; Matsuo, J. *Appl. Surf. Sci.* **2008**, *255*, 1588–1590.
16. Sheraz nee Rabbani, S.; Barber, A.; Fletcher, J. S.; Lockyer, N. P.; Vickerman, J. C. *Anal. Chem.* **2013**, *85*, 5654–5658.
17. Lee, P. L.; Chen, B. C.; Gollavelli, G.; Shen, S. Y.; Yin, Y. S.; Lei, S. L.; Jhang, C. L.; Lee, W. R.; Ling, Y. C. *J. Hazard. Mater.* **2014**, *277*, 3–12.
18. Kurczy, M. E.; Piehowski, P. D.; Parry, S. A.; Jiang, M.; Chen, G.; Ewing, A. G.; Winograd, N. *Appl. Surf. Sci.* **2008**, *255*, 1298–1304.
19. Cannon, D. M.; Michaeleen, J.; Pacholski, L.; Winograd, N.; Ewing, A. E. *J. Am. Chem. Soc.* **2000**, *122*, 603–610.
20. Passarelli, M. K.; Winograd, N. *Biochim. Biophys. Acta* **2011**, *1811*, 976–990.
21. Brison, J.; Benoit, D. S.; Muramoto, S.; Robinson, M.; Stayton, P. S.; Castner, D. G. *Surf. Interface Anal.* **2011**, *43*, 354–357.
22. Nagata, Y.; Ishizaki, I.; Waki, M.; Ide, Y.; Hossen, M. A.; Ohnishi, K.; Sanada, N.; Setou, M. *Surf. Interface Anal.* **2014**.
23. Kurczy, M. E.; Piehowski, P. D.; Van Bell, C. T.; Heien, M. L.; Winograd, N.; Ewing, A. G. *Proc. Natl. Acad. Sci. U. S. A.* **2010**, *107*, 2751–2756.
24. Ostrowski, S. G.; Van Bell, C. T.; Winograd, N.; Ewing, A. G. *Science* **2004**, *305*, 71–73.
25. Chandra, S.; Harris, W. C.; Morrison, G. H. *J. Histochem. Cytochem.* **1984**, *32*, 1224–1230.
26. Chandra, S.; Ausserer, W. A.; Morrison, G. H. *J. Cell Sci.* **1992**, *102*, 417–425.
27. Smith, D. R.; Chandra, S.; Barth, R. F.; Yang, W.; Joel, D. D.; Coderre, J. A. *Cancer Res.* **2001**, *61*, 8179–8187.
28. Chandra, S.; Smith, D. R.; Morrison, G. H. *Anal. Chem.* **2000**, *72*, 104A–114A.
29. Slodzian, G.; Daigne, B.; Girard, F.; Boust, F.; Hillion, F. *Biol. Cell.* **1992**, *74*, 43–50.
30. Lechene, C.; Hillion, F.; McMahon, G.; Benson, D.; Kleinfeld, A. M.; Kampf, J. P.; Distel, D.; Luyten, Y.; Bonventre, J.; Hentschel, D.; Park, K. M.; Ito, S.; Schwartz, M.; Benichou, G.; Slodzian, G. J. *Biology* **2006**, *5*, 20.1–20.30.
31. McMahon, G.; Glassner, B. J.; Lechene, C. P. *Appl. Surf. Sci.* **2006**, *252*, 6895–6906.
32. Grovenor, C. R. M.; Smart, K. E.; Kilburn, M. R.; Shore, B.; Dilworth, J. R.; Martin, B.; Hawes, C.; Rickaby, R. E.M *Appl. Surf. Sci.* **2006**, *252*, 6917–6924.
33. Steinhauser, M. L.; Bailey, A. P.; Senyo, S. E.; Guillermier, C.; Perlstein, T. S.; Gould, A. P.; Lee, R. T.; Lechene, C. P. *Nature* **2012**, *481*, U131–U516.
34. Zhang, D. S.; Piazza, V.; Perrin, B. J.; Rzadzinska, A. K.; Poczatek, J. C.; Wang, M.; Prosser, H. M.; Ervasti, J. M.; Corey, D. P.; Lechene, C. P. *Nature* **2012**, *481*, U137–U520.
35. Senyo, S. E.; Steinhauser, M. L.; Pizzimenti, C. L.; Yang, V. K.; Cai, L.; Wang, M.; Wu, T. D.; Guerquin-Kern, J. L.; Lechene, C. P.; Lee, R. T. *Nature* **2013**, *493*, 433–436.
36. Kamal, M. M.; Mills, D.; Grzybek, M.; Howard, J. *Proc. Natl. Acad. Sci. U.S.A.* **2009**, *106*, 22245–22250.
37. Hao, M.; Mukherjee, S.; Maxfield, F. R. *Proc. Natl. Acad. Sci. U. S. A.* **2001**, *98*, 13072–13077.
38. Frisz, J. F.; Lou, K.; Klitzing, H. A.; Hanafin, W. P.; Lizunov, V.; Wilson, R. L.; Carpenter, K. J.; Kim, R.; Hutcheon, I. D.; Zimmerberg, J.; Weber, P. K.; Kraft, M. L. *Proc. Natl. Acad. Sci. U. S. A.* **2013**, *110*, E613–E622.
39. Legin, A. A.; Schintlmeister, A.; Jakupec, M. A.; Galanski, M.; Lichtscheidl, I.; Wagner, M.; Keppler, B. K. *Chem. Sci.* **2014**, *5*, 3135.

40. Fletcher, J. S.; Vickerman, J. C. *Anal. Bioanal. Chem.* **2010**, *396*, 85–104.
41. Seeley, E. H.; Caprioli, R. M. *Anal. Chem.* **2012**, *84*, 2105–2110.
42. Eberlin, L. S.; Ifa, D. R.; Wu, C.; Cooks, R. G. *Angew. Chem.* **2010**, *49*, 873–876.
43. Fletcher, J. S.; Rabbani, S.; Henderson, A.; Lockyer, N. P.; Vickerman, J. C. *Rapid Commun. Mass Spectrom.* **2011**, *25*, 925–932.
44. Brison, J.; Robinson, M. A.; Benoit, D. S.; Muramoto, S.; Stayton, P. S.; Castner, D. G. *Anal. Chem.* **2013**, *85*, 10869–10877.
45. Angerer, T. B.; Fletcher, J. S. *Surf. Interface Anal.* **2014**.
46. Jurchen, J. C.; Rubakhin, S. S.; Sweedler, J. V. *J. Am. Soc. Mass Spectrom.* **2005**, *16*, 1654–1659.
47. Luxembourg, S. L.; Mize, T. H.; McDonnell, L. A.; Heeren, R. M. A. *Ana. Chem.* **2004**, *76*, 5339–5344.
48. Zavalin, A.; Todd, E. M.; Rawhouser, P. D.; Yang, J.; Norris, J. L.; Caprioli, R. M. *J. Mass Spectrom.* **2012**, *47*, 1473–1481.
49. Guenther, S.; Koestler, M.; Schulz, O.; Spengler, B. *Int. J. Mass Spectrom.* **2010**, *294*, 7–15.
50. Cillero-Pastor, B.; Heeren, R. M. *J. Proteome Res.* **2014**, *13*, 325–335.
51. Thomas, A.; Chaurand, P. *Bioanalysis* **2014**, *6*, 967–982.
52. Chiang, C. K.; Chen, W. T.; Chang, H. T. *Chem. Soc. Rev.* **2011**, *40*, 1269–1281.
53. Dufresne, M.; Thomas, A.; Breault-Turcot, J.; Masson, J. F.; Chaurand, P. *Anal. Chem.* **2013**, *85*, 3318–3324.
54. Taira, S.; Sugiura, Y.; Moritake, S.; Shimma, S.; Ichiyanagi, Y.; Setou, M. *Anal. Chem.* **2008**, *80*, 4761–4766.
55. Bouschen, W.; Schulz, O.; Eikel, D.; Spengler, B. *Rapid Commun. Mass Spectrom.* **2010**, *24*, 355–364.
56. Schober, Y.; Guenther, S.; Spengler, B.; Rompp, A. *Anal. Chem.* **2012**, *84*, 6293–6297.
57. Rubakhin, S. S.; Greenough, W. T.; Sweedler, J. V. *Anal. Chem.* **2003**, *75*, 5374–5380.
58. Thiery-Lavenant, G.; Zavalin, A. I.; Caprioli, R. M. *J. Am. Soc. Mass Spectrom.* **2013**, *24*, 609–614.
59. Oetjen, J.; Aichler, M.; Trede, D.; Strehlow, J.; Berger, J.; Heldmann, S.; Becker, M.; Gottschalk, M.; Kobarg, J. H.; Wirtz, S.; Schiffler, S.; Thiele, H.; Walch, A.; Maass, P.; Alexandrov, T. *J. Proteomics* **2013**, *90*, 52–60.
60. Chughtai, K.; Jiang, L.; Greenwood, T. R.; Klinkert, I.; Amstalden van Hove, E. R.; Heeren, R. M.; Glunde, K. *Anal. Chem.* **2012**, *84*, 1817–1823.
61. Thiele, H.; Heldmann, S.; Trede, D.; Strehlow, J.; Wirtz, S.; Dreher, W.; Berger, J.; Oetjen, J.; Kobarg, J. H.; Fischer, B.; Maass, P. *Biochim. Biophys. Acta* **2014**, *1844*, 117–137.
62. Rubakhin, S. S.; Lanni, E. J.; Sweedler, J. V. *Curr. Opin. Biotechnol.* **2013**, *24*, 95–104.
63. Heinemann, M.; Zenobi, R. *Curr. Opin. Biotechnol.* **2011**, *22*, 26–31.
64. Svatos, A. *Anal. Chem.* **2011**, *83*, 5037–5044.
65. Winograd, N. *Anal. Chem.* **2005**, *1*, 143A–149A.
66. Benninghoven, A. *Angew. Chem.* **1994**, *33*, 1023–1043.
67. Venter, A.; Nefliu, M.; Graham Cooks, R. *Trends Anal. Chem.* **2008**, *27*, 284–290.
68. Chen, C. T.; Chen, Y. C. *Anal. Chem.* **2005**, *77*, 5912–5919.
69. Takats, Z.; Wiseman, J. M.; Cooks, R. G. *J. Mass Spectrom.* **2005**, *40*, 1261–1275.
70. Yang, J.; Caprioli, R. M. *Anal. Chem.* **2011**, *83*, 5728–5734.
71. Altelaar, A. F. M.; Taban, I. M.; McDonnell, L. A.; Verhaert, P. D. E. M.; de Lange, R. P. J.; Adan, R. A. H.; Mooi, W. J.; Heeren, R. M. A.; Piersma, S. R. *Int. J. Mass Spectrom.* **2007**, *260*, 203–211.
72. Rompp, A.; Spengler, B. *Histochem. Cell Biol.* **2013**, *139*, 759–783.
73. Costa, A. B.; Graham Cooks, R. *Chem. Phys. Lett.* **2008**, *464*, 1–8.
74. Campbell, D. I.; Ferreira, C. R.; Eberlin, L. S.; Cooks, R. G. *Anal. Bioanal. Chem.* **2012**, *404*, 389–398.
75. Roach, P. J.; Laskin, J.; Laskin, A. *Analyst* **2010**, *135*, 2233–2236.
76. Laskin, J.; Heath, B. S.; Roach, P. J.; Cazares, L.; Semmes, O. J. *Anal. Chem.* **2012**, *84*, 141–148.
77. Bodzon-Kulakowska, A.; Drabik, A.; Marszalek, M.; Kotlinska, J. H.; Suder, P. *J. Mass Spectrom.* **2014**, *49*, 613–621.
78. Angerer, T. B.; Blenkinsopp, P.; Fletcher, J. S. *Int. J. Mass Spectrom.* **2014**.